Supplementary Information

Ultra robust negative differential resistance memristor for hardware neuron circuit implementation

Yifei Pei[1], Biao Yang[2], Xumeng Zhang[3], Hui He[1], Yong Sun[2], Jianhui Zhao[2], Pei Chen[3], Zhanfeng Wang[1], Niefeng Sun[4] Shixiong Liang[5], Guodong Gu[4], Qi Liu[*3], Shushen Li[1,6]& Xiaobing Yan[*1,2]

[1]Key Laboratory of Brain like Neuromorphic Devices and Systems of Hebei Province, College of Physics Science and Technology, Hebei University, Baoding 071002, Hebei, China.

[2]College of Electronic and Information Engineering, Hebei University, Baoding 071002, China.

[3]Frontier Institute of Chip and System, Fudan University, Shanghai 200433, China.

[4]National Key Laboratory of Solid-state Microwave Devices and Circuits, Hebei Semiconductor Research Institute, Shijiazhuang 050051, China.

[5]School of Microelectronics, Tianjin University, Tianjin 300072, China.

[6]State Key Laboratory of Superlattices and Microstructures, Institute of Semiconductors, Chinese Academy of Sciences, P.O. Box 912, Beijing, 100083, China.

These authors contributed equally: Yifei Pei, Biao Yang, Xumeng Zhang.

e-mail: yanxiaobing@ime.ac.cn

qi_liu@fudan.edu.cn

Contents:

Section 1: Detailed description

1.1. Principle of negative differential resistance

State 1. In the equilibrium state (no voltage), the system has a uniform Fermi level, which means that neither electrons nor holes have quantum states with the same energy. As a result, the current in the system is zero.

State 2. When a small voltage is applied to the device, the energy band in the N region is raised, allowing electrons below the Fermi level in the N region to access quantum states of equal energy in the P region. This results in electron tunneling and the generation of a forward tunneling current.

State 3. As the voltage increases, the energy band in the N region rises further, enabling more electrons below the Fermi level in the N region to have corresponding quantum states, thus increasing the tunneling current. When the Fermi level in the N region rises to the same level as the top of the valence band in the P region, the tunneling current reaches its maximum value.

State 4. As the voltage continues to increase, the Fermi level in the N region rises further, and the number of quantum states with the same energy as the electrons in the N region decreases, causing the tunneling current to gradually decrease. When the bottom of the conduction band in the N region aligns with the top of the valence band in the P region, the current of the device reaches its minimum value.

State 5. With a further increase in voltage, due to the smaller potential barrier between the P and N regions, the diffusion current of the device increases, leading to an overall increase in the device's current.

State 6. As the voltage starts to decrease, the diffusion current gradually reduces, and the current begins to decline. Due to internal defects in semiconductor materials that can capture electrons, there is an accumulation of electrons at the interface. When the current decreases, the captured electrons are released, resulting in a hysteresis phenomenon.

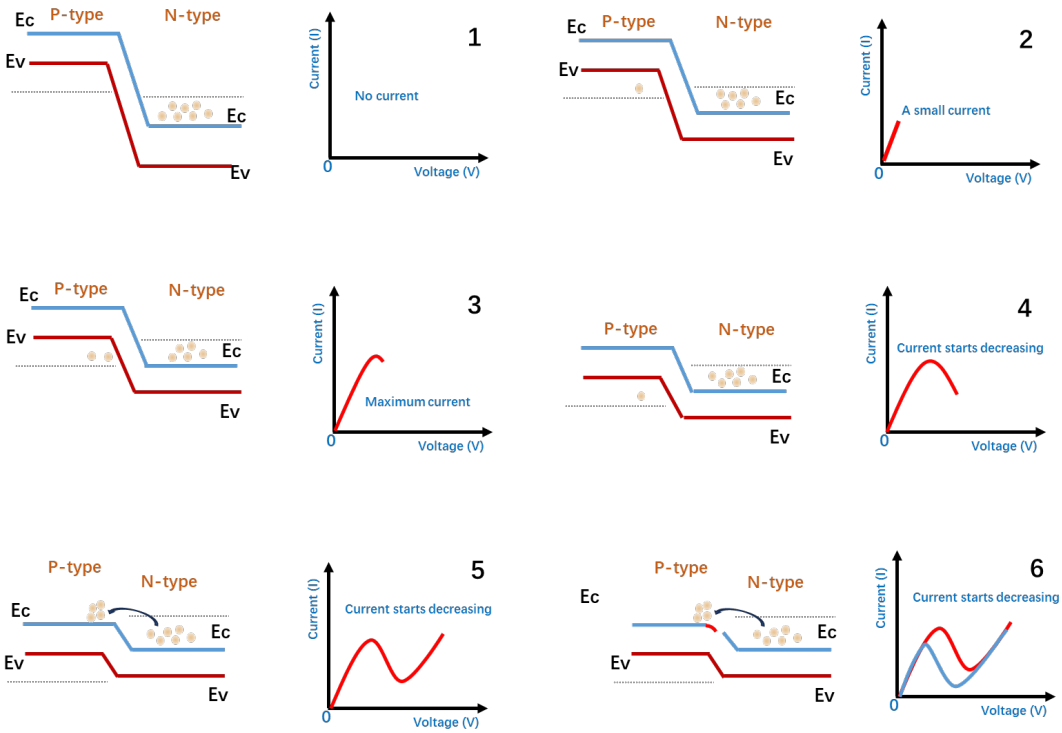

Figure 1. Working steps of NDR devices.

1.2 The 9 neuron behaviors

Phasic spiking

A neuron may only emit one pulse at the beginning of input, and then remain stationary. This response is called a phase spike and is useful for detecting the onset of stimuli.

Anodal break excitation

When the input suddenly increases, this spike of biological neurons is called anode break excitation.

Spike accommodation

If the rising time is long, there will be no spike. This kind of biological neuron characteristic that produces spike when input increases in a short time is called spike accommodation.

Subthreshold oscillations

Each brain structure has neurons capable of displaying oscillatory potentials. The frequency of this oscillation plays an important role, and these neurons act as band-pass filters.

Class 1 excitable

The frequency of the tension spike of the RS excitatory neurons in the neocortex depends on the intensity of the input. When the input is weak (but beyond the threshold), the ability to stimulate the low-frequency spike is called Class 1 excitability. Class 1 excitability neurons can

encode the input intensity as their discharge rate.

All or nothing firing

It is either firing, or it is completely off, and no output is produced.

Tonic bursting

Some neurons, such as the chattering neurons in cat neocortex, fire periodic bursts of spikes when stimulated. It is believed that such neurons contribute to the gamma frequency oscillation in the brain.

Refractory period

The refractory period of a neuron is the time in which a nerve cell is unable to fire an action potential (nerve impulse).

Accommodation

Neurons are extremely sensitive to brief coincident inputs but may not fire in response to a strong but slowly increasing input. The slowly ramped current in the figure does not elicit a spike, while a smaller but sharply ramped current elicits a spike. During the slow ramp, the inward currents have enough time to inactivate, and outward currents have enough time to activate, so the neuron accommodates, becomes less excitable and cannot generate a spike.

1.3 SSIM and PSNR

SSIM

The full name of SSIM is structural similarity index, which is a measure of the similarity of two images. The specific calculation process is as follows

$$SSIM(x,y) = [l(x,y)]^{\alpha} * [c(x,y)]^{\beta} * [s(x,y)]^{\gamma}$$

$$l(x,y) = \frac{2\mu_x\mu_y + C_1}{{\mu_x}^2 + {\mu_y}^2 + C_1}$$

$$c(x,y) = \frac{2\sigma_x\sigma_y + C_2}{{\sigma_x}^2 + {\sigma_y}^2 + C_2}$$

$$s(x,y) = \frac{\sigma_{xy} + C_3}{\sigma_x\sigma_y + C_3}$$

μ_x and μ_y are the means of images X and Y, respectively, σ_x and σ_y are the standard deviations of images X and Y, respectively, and σ_{xy} denotes the covariance of images X and Y. Usually $C_1 = (K_1L)^2, C_2 = (K_2L)^2, C_3 = C_2/2,$ the $K_1 = 0.01, K_2 = 0.03, L = 255$. SSIM values are between 0 and 1, the closer to 1, the more similar the two images are.

PSNR

The peak signal-to-noise ratio (PSNR) is the logarithmic value of the mean-square error between two images relative to $(\mathrm{MaxValue})^2$, MaxValue is the maximum value of the pixel value. It is measured in dB, the larger the value, the closer the two images are.

2.4 Processing of data sets

The ten categories in the MNIST dataset were divided equally, with half of them labelled 175°C and the other 325°C, to form a new twenty-category dataset. When converted into spikes signals by neurons, the voltage frequency response curves at different temperatures are called according to the temperature labels of the handwritten digital images, while the pixel values of the images are mapped to the input voltages, and the frequency mapping diagrams of some of the datasets processed by the FN neurons are shown in Fig. S18

Section 3: Supplementary Figure

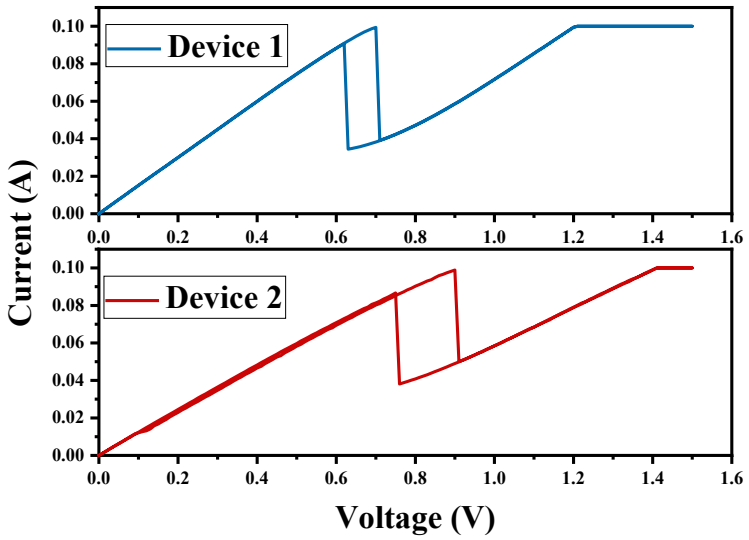

Figure S1. The two I-V characteristic curves under voltage force.

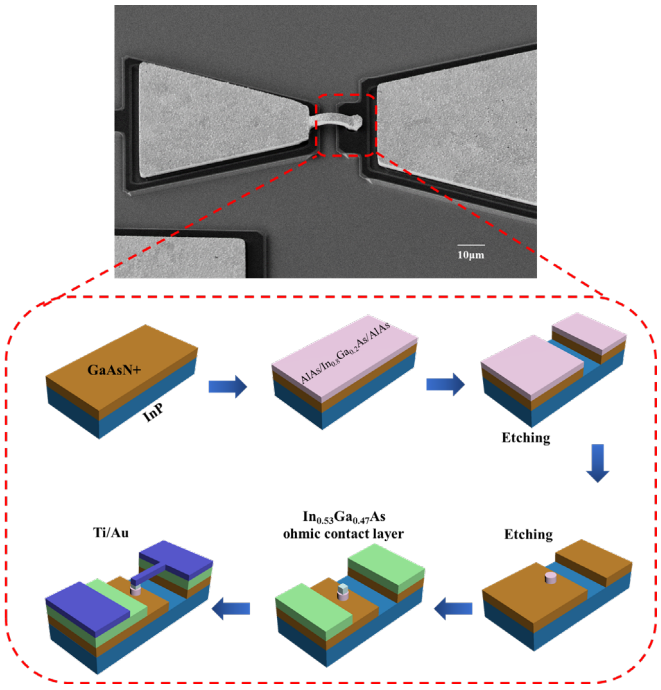

Figure S2. Process flowchart of NDR device preparation.

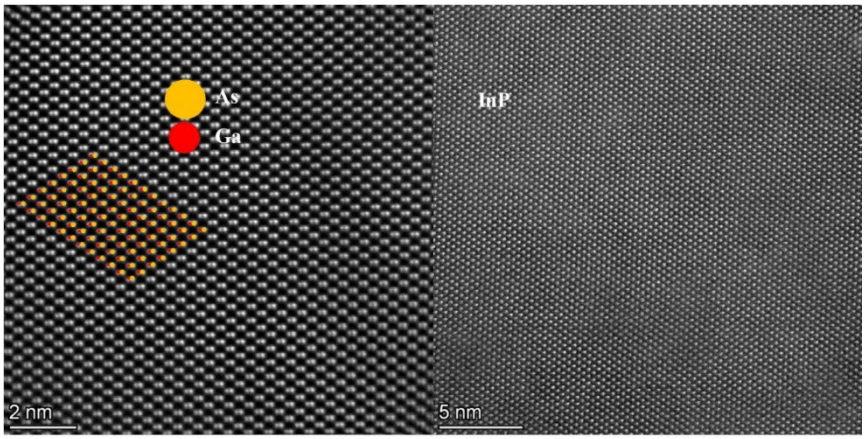

Figure S3. High resolution TEM images of InP and GaAs.

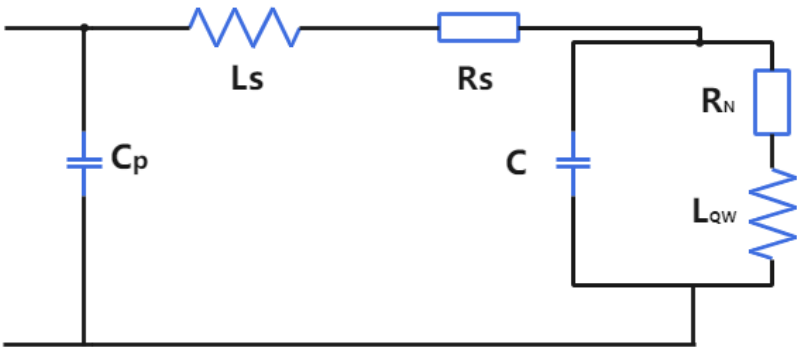

Figure S4. Equivalent circuit model of NDR device.

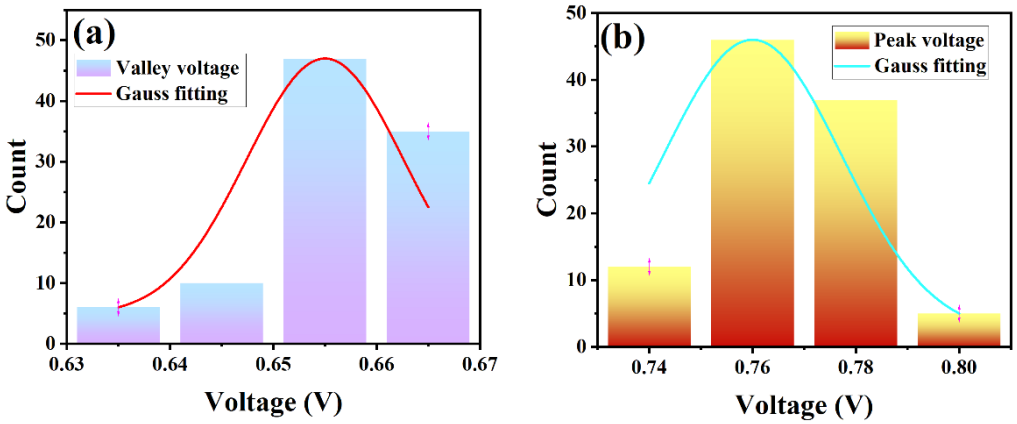

Figure S5. a, Statistical data of Gaussian fitted histograms of peak voltage of devices. b, Statistical data of Gaussian fitted histograms of valley voltage of devices.

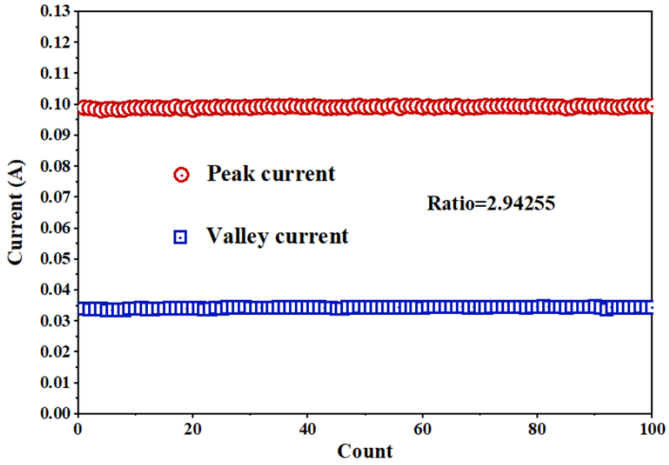

Figure S6. According to the statistics of peak current and valley current in 100 cycles, the ratio of peak to valley current is about 2.94.

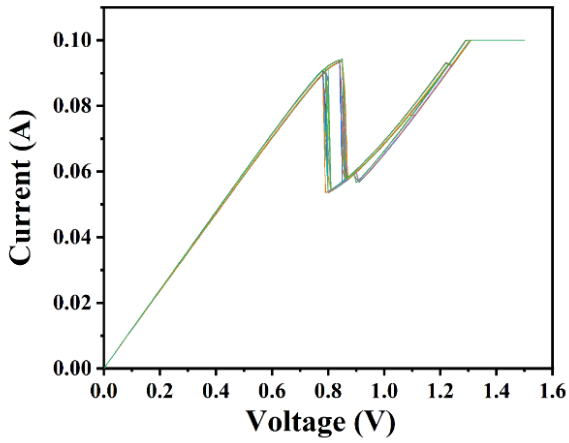

Figure S7. The 100 cycles of I-V cycles of the device at 400 ℃

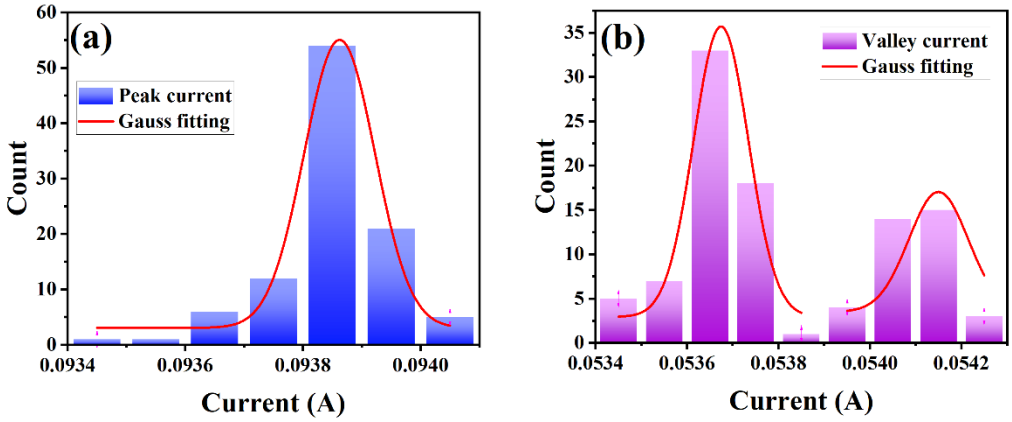

Figure S8. a, The statistical data of Gaussian fitting histogram of valley current at 400 ℃. b, The statistical data of Gaussian fitting histogram of peak current at 400 ℃.

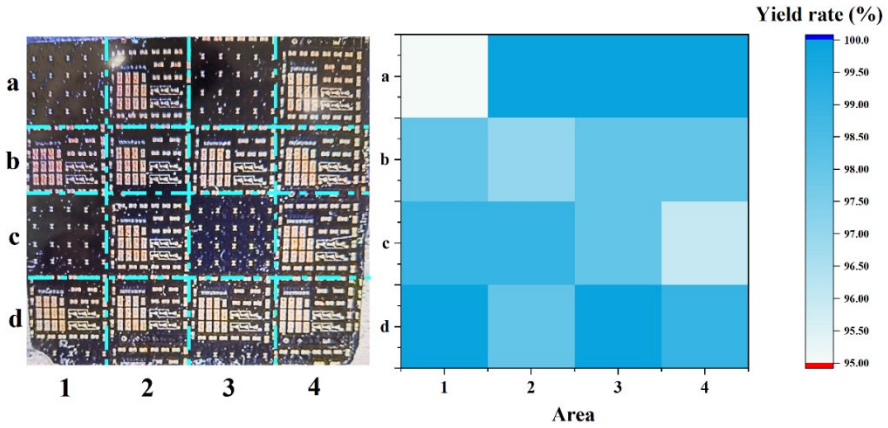

Figure S9. The yield of components under different graphical conditions.

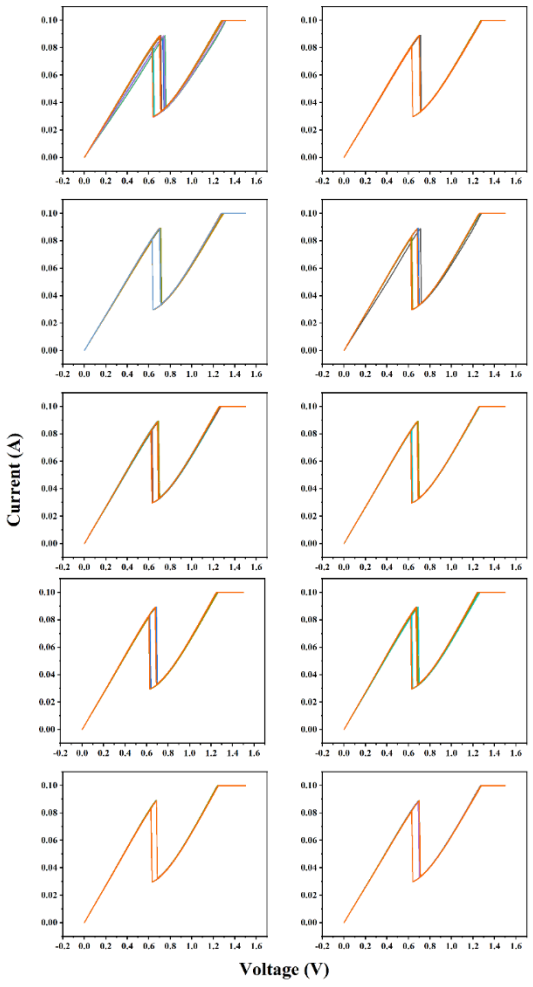

Figure S10. I-V characteristic cycle of NDR devices for different batches.

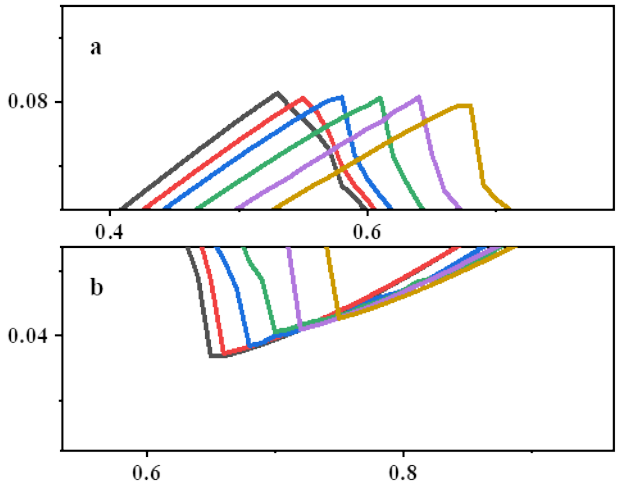

Figure S11. **a**, At different temperatures, the peak I-V amplifies the image. With the increase of temperature, the peak voltage increases gradually, and the current has no obvious change. **b**, The valley value I-V enlarges the image at different temperatures. With the increase of temperature, the valley voltage and current increase gradually.

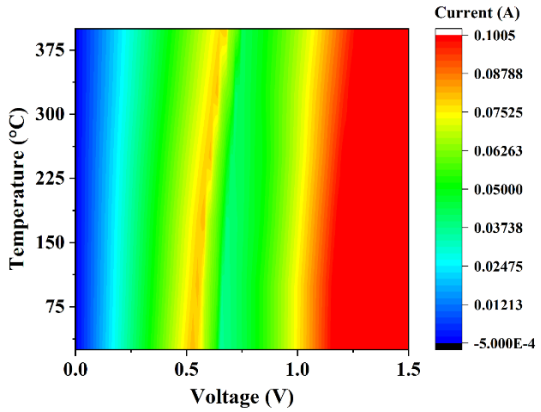

Figure S12. The relationship between voltage and current and temperature.

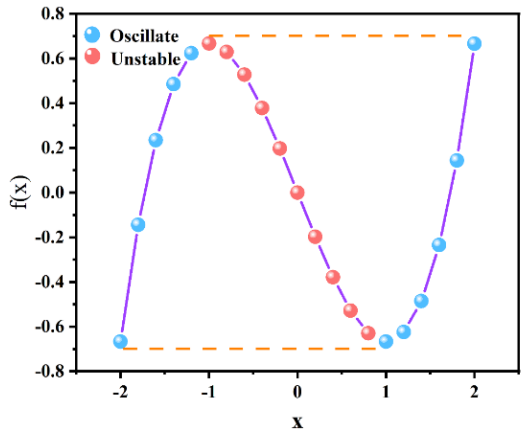

Figure S13. In the FN neuron model, f (x)=-x+x^3/3 function image.

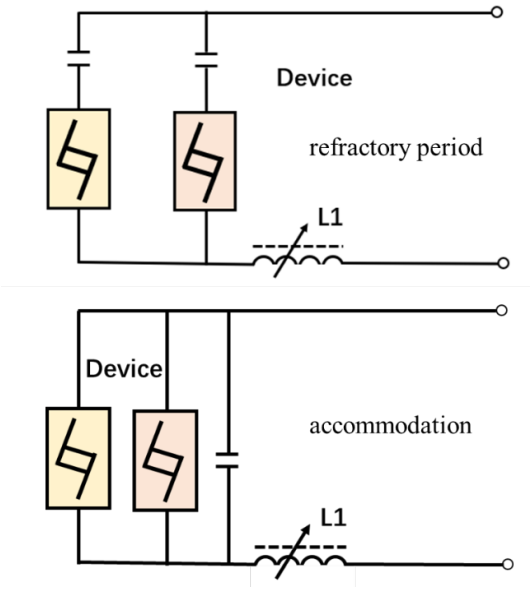

Figure S14. The circuit of the accommodation which improved based on Figure 1.

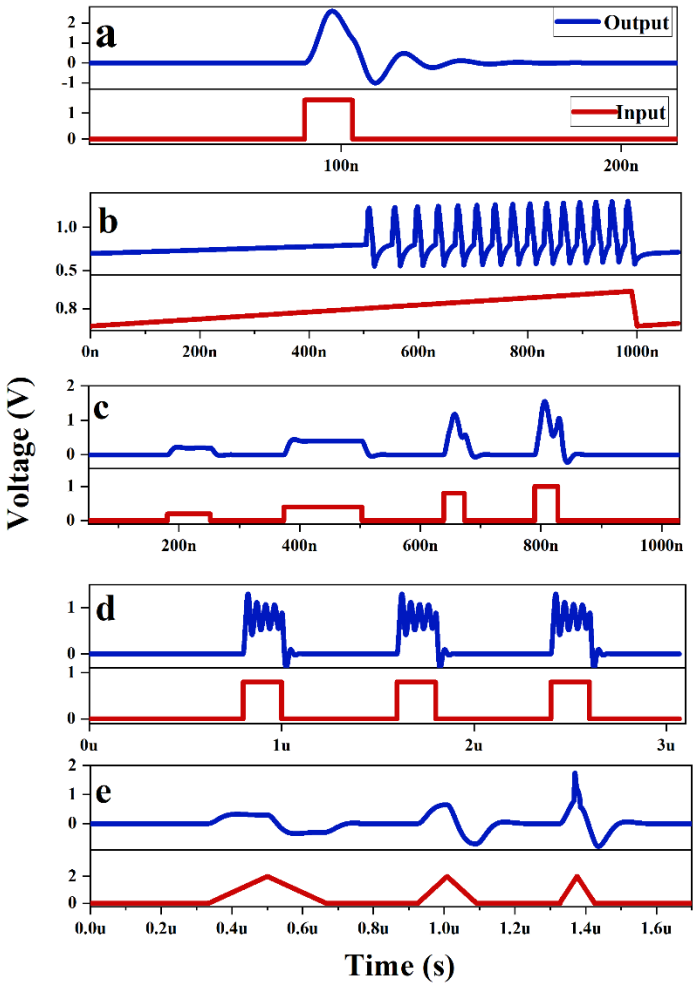

Figure S15. Simulation results of FN neuron behavior software. a, Phasic spiking. b, Class 1 excitable. c, All-or-nothing firing. d, Tonic bursting. e, Accommodation.

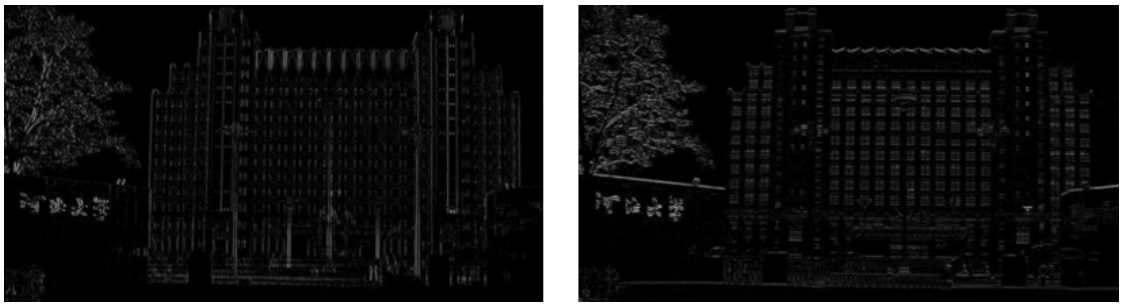

Figure S16. Detection results along the XY direction, respectively, the left figure shows the X direction and the right figure shows the Y direction.

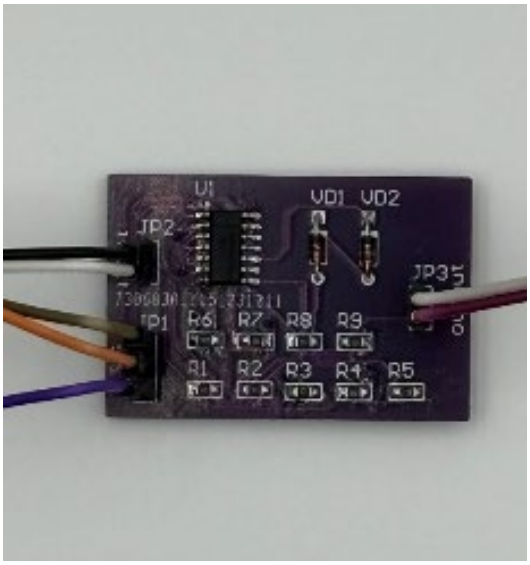

Figure S17. PCB for processing unit.

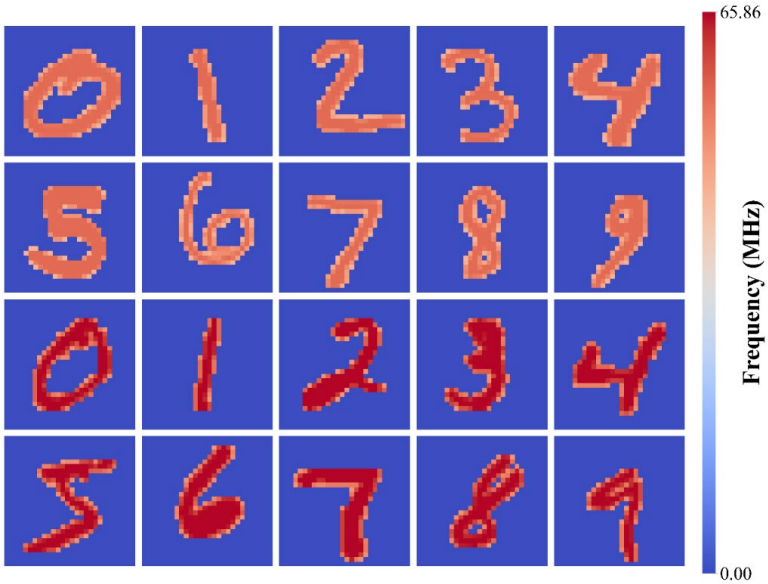

Figure S18. Twenty classes of digital images with different temperature labels processed by FN neurons, the first two classes with 175°C and the last two classes with 325°C.

Section 4: Supplementary Table

Table S1. Comparison of performance with threshold switching devices used in neural circuits in recent years.

Material system	Endurance	Variation	Neuronal complexity	Turn-on time	Turn-off time	Ref
$Ag/SiO_2/Au$	-		3	-	-	1
$Au/VO_2/Au$	6.5×10^6	0.73%	3	<70ns	<60ns	2
$Pt/Ti/NbO_x/Pt/Ti$	50		2	<50ns	<25ns	3
Pt/CuS/GeSe/Pt	1.8×10^6		3	200ns	~3μs	4
$Pd/Ag/HfO_x/Ag/Pd$	1×10^8			75ns	250ns	5
$Ag/ZrO_x/Pt$	200	5.56%	-	-	-	6
Au/Ag/hBN/Au/Ti	500	37.5%	3	-	-	7
$Ag/WSe_2/Ag$	1×10^4		-	700ns	-	8
$Au/CH_3NH_3PbI_3/ITO$	-		8	-	-	9
$Pt/VO_2/Pt$	2.66×10^7		4	-	-	10
$Pt/PEDOT:PSS/WO_3/W$	-		4	-	-	11
$Pt/SiO_2(Ag)/SiO_2/Pt$	-		3		<1ms	12
$Pt/Ti/NbO_x/Pt$	-		2	-	-	13
$Pt/AgGeSe/Al_2O_3/Pt$	-	2.18%	-	<300ns	<30μs	14
$Ag/TiN/HfO_x/HfO_y/HfO_z/Pt$	1×10^6	5.4%	-	60ns	500ns	15
Ag/Si/Pt	-		3	20ns	16ns	16
This work	1×10^{11}	0.295%	1	10ns	50ns	

Table S2. The similarity between this circuit and the FN neurons in the model.

FN neuron model	Neuron equivalent in proposed NDR-based circuit
Injected current, z	I_L
Neuron membrane potential, x	V_L
Recovery variable, y	V_{valley}
$-x+\frac{x^3}{3}+\frac{dx}{cdt}$	$I_1+I_2=I_L$

Table S3. Compared to the complexity of neural circuits in other works.

Number of components	Neuron model	Neurons Active	Ref.
1 PCM + reset circuit	Stochastic IF	1	17
14FETs + 2 capacitors	IF	4	18
1MTJ+reset circuit	Stochastic IF	2	19
>100FETs+2 capacitors	FN		20
2 memristor+ 2 capacitors+ 2 resistor	HH	23	10
1 capacitors+1 resistor+1memristor	LIF	1	21
2 NDR+ 1 inductance	FN	9	This work

References

1 Zhang, X. *et al.* An artificial neuron based on a threshold switching memristor. *IEEE Electron Device Letters* **39**, 308-311 (2017).

2 Yuan, R. *et al.* A neuromorphic physiological signal processing system based on VO2 memristor for next-generation human-machine interface. *Nature Communications* **14**, 3695 (2023).

3 Duan, Q. *et al.* Spiking neurons with spatiotemporal dynamics and gain modulation for monolithically integrated memristive neural networks. *Nature communications* **11**, 3399 (2020).

4 Wang, K. *et al.* Threshold switching memristor-based stochastic neurons for probabilistic computing. *Materials Horizons* **8**, 619-629 (2021).

5 Midya, R. *et al.* Anatomy of Ag/Hafnia-based selectors with 10 10 nonlinearity. *Advanced Materials* **29** (2017).

6 Yang, J. H., Mao, S. C., Chen, K. T. & Chen, J. S. Emulating Nociceptive Receptor and LIF Neuron Behavior via ZrOx-based Threshold Switching Memristor. *Advanced Electronic Materials* **9**, 2201006 (2023).

7 Jo, Y. *et al.* Hardware Implementation of Network Connectivity Relationships Using 2D hBN-

Based Artificial Neuron and Synaptic Devices. *Advanced Functional Materials* **34**, 2309058 (2024).

8 Sivan, M. *et al.* All WSe2 1T1R resistive RAM cell for future monolithic 3D embedded memory integration. *Nature communications* **10**, 5201 (2019).

9 Yang, J.-Q. *et al.* Leaky integrate-and-fire neurons based on perovskite memristor for spiking neural networks. *Nano Energy* **74**, 104828 (2020).

10 Yi, W. *et al.* Biological plausibility and stochasticity in scalable VO2 active memristor neurons. *Nature communications* **9**, 4661 (2018).

11 Huang, H. M. *et al.* Quasi-Hodgkin–Huxley Neurons with Leaky Integrate-and-Fire Functions Physically Realized with Memristive Devices. *Advanced Materials* **31**, 1803849 (2019).

12 Ye, F., Kiani, F., Huang, Y. & Xia, Q. Diffusive Memristors with Uniform and Tunable Relaxation Time for Spike Generation in Event-Based Pattern Recognition. *Advanced Materials* **35**, 2204778 (2023).

13 Kim, G. *et al.* Self-clocking fast and variation tolerant true random number generator based on a stochastic mott memristor. *Nature communications* **12**, 2906 (2021).

14 Wan, T.-Q. *et al.* 12.7 MA/cm 2 on-current density and high uniformity realized in AgGeSe/Al 2 O 3 selectors. *IEEE Electron Device Letters* **42**, 613-616 (2021).

15 Lu, Y. F. *et al.* A high-performance Ag/TiN/HfOx/HfOy/HfOx/Pt diffusive memristor for calibration-free true random number generator. *Advanced Electronic Materials* **8**, 2200202 (2022).

16 Yan, L. *et al.* High-speed Si films based threshold switching device and its artificial neuron application. *Applied Physics Letters* **119** (2021).

17 Tuma, T., Pantazi, A., Le Gallo, M., Sebastian, A. & Eleftheriou, E. Stochastic phase-change neurons. *Nature nanotechnology* **11**, 693-699 (2016).

18 Wijekoon, J. H. & Dudek, P. Compact silicon neuron circuit with spiking and bursting behaviour. *Neural Networks* **21**, 524-534 (2008).

19 Sengupta, A., Panda, P., Wijesinghe, P., Kim, Y. & Roy, K. Magnetic tunnel junction mimics stochastic cortical spiking neurons. *Scientific reports* **6**, 30039 (2016).

20 Khanday, F. A., Kant, N. A., Dar, M. R., Zulkifli, T. Z. A. & Psychalinos, C. Low-voltage low-power integrable CMOS circuit implementation of integer-and fractional–order FitzHugh–Nagumo neuron model. *IEEE Transactions on Neural Networks and Learning Systems* **30**, 2108-2122 (2018).

21 Zhang, X. *et al.* An artificial spiking afferent nerve based on Mott memristors for neurorobotics. *Nature communications* **11**, 51 (2020).